Advances in Engineering Software 119 (2018) 103–115

Contents lists available at ScienceDirect

Advances in Engineering Software

journal homepage: www.elsevier.com/locate/advengsoft

Research paper

An adaptive isogeometric boundary element method for predicting the effective thermal conductivity of steady state heterogeneity

Y.P. Gong, C.Y. Dong*, X.Y. Qu

Department of Mechanics, School of Aerospace Engineering, Beijing Institute of Technology, Beijing 100081, China

ARTICLE INFO

Keywords:
IGBEM
GSCS
Effective thermal conductivity
Adaptive integration method

ABSTRACT

This work presents an adaptive isogeometric boundary element method (IGBEM) for the calculation of effective thermal conductivity of steady state heterogeneities. Based on the generalized self-consistent scheme (GSCS), some integral equation formulations which only contain the unknown temperatures on the interface are used to calculate the effective thermal conductivity of steady state composites. In our approach, the geometries of the inclusion and original matrix are described using NURBS basis functions. The advantage over currently used methods is that no geometrical errors exist in the analysis process. And the geometry data in the isogeometric GSCS model can be taken directly from CAD programs. In addition, based on the upper bound of the relative error of the Gaussian quadrature formula, an adaptive integration method is used to compute the boundary integrals, which makes the computation of the integrals easier and more efficient at optimal computational cost. The comparisons between the results obtained by the present method and the existing counterparts are carried out and the good agreement can be observed.

1. Introduction

Composite materials are being used increasingly in a variety of modern engineering applications and this trend is likely to continue. The reason is that many composite materials possess a number of highly desirable engineering properties that can be exploited to design structures with high demand on their performance. Therefore, analysis of the effective properties of composite materials has received considerable attention in scientific community [1]. Many theoretical models, such as differential scheme [2], modified Eshelby's model (MEM) [3], self-consistent method (SCM) [4] and the generalized self-consistent scheme (GSCS) [5], for predicting the effective properties of composites have been presented. In [6,7], the SCM was applied to a composite reinforced with spherical fillers, which determines the elastic constants of the composite by embedding only one filler into an infinite domain with the composite property determined. The GSCS, closely related with the SCM, has been proposed by Christen and Lo [5]. Main idea of the GSCS is in the assumption that the particle surrounded by the matrix material is embedded in an effective medium of unknown properties. This method can yield better results than the SCM [8].

The finite element analysis of the GSCS for solving the elastic-plastic heterogeneous problems, inverse problems and mechanical degradation of fibrous composites was carried out by Lefik et al. [9] and Boso et al. [10,11]. This method is based on two separated finite element models, i.e. a fine heterogeneous model and a coarse homogeneous model. The effective material properties of a coarse homogeneous model are iteratively computed enough to close the response of the fine heterogeneous. The disadvantage of this method is that it requires to discretize the whole computation domain and more fine meshes near the interfaces, i.e. the inclusion and the original matrix as well as the original matrix and the effective matrix, are needed. Therefore, a huge computer memory is needed to store the related finite element information. And lots of computer execution time is required to calculate the effective properties of composited material. Due to the merits of high accuracy and only the boundary description of the problem, the boundary element method (BEM) has been widely used to deal with the thermal conduction problems [12–13]. In [12], each region with different heat transfer properties was taken as a piecewise homogeneous in a heterogeneous medium. The resulting non-square global system matrix was solved by the singular value decomposition method. In [13], some new integral equation formulations suitable for steady state thermal conduction were presented to calculate the effective thermal conductivity of steady state problems. These equations only contain the unknown temperatures on the interface. Boundary face method was used to deal with thermal conduction problems in [14]. And a large number of open-ended tubular shaped holes of small diameters were studied. In numerical process, a new meshing scheme was adopted to discretize the holes of which the exact geometry remained.

* Corresponding author.
E-mail address: cydong@bit.edu.cn (C.Y. Dong).

https://doi.org/10.1016/j.advengsoft.2018.03.001
Received 28 May 2017; Received in revised form 22 October 2017; Accepted 3 March 2018

In 2005, Hughes et al. proposed the ``Isogeometric Analysis" (IGA) paradigm [15] as a means to perform finite element analysis directly from computer aided design data, for three-dimensional regions. The first paper known to the authors to propose isogeometric approximations dates back to 1982 [16], although the approach was significantly different from the 2005 paper of Hughes et al. Several methods were later devised in order to alleviate the difficulties existed in the original version of IGA. Particularly the lack of an automatic parameterisation to build the approximation within the domain was addressed through (a) special parameterisation techniques, for example based on variational harmonic methods [17]. Xu et al. proposed a method to parameterize the computational domains [18]. Xu et al. also devised analysis-aware parameterisation methods for single [19] and multi-domain geometries [20]. The stability issues associated with parameterization was studied in [21]. (b) geometry independent field approximation (GIFT) where the spline spaces used for the geometry and the field variables can be chosen and adapted independently while preserving geometric exactness and tight CAD integration [22]. (c) isogeometric boundary element methods (IGBEM), proposed in [23,24] and was later generalized to 3D T-spline geometries in [25]. IGBEM allows stress analysis directly from CAD, without any mesh generation or regeneration [26] and was recently used for damage tolerance assessment of complex structures, directly from CAD [27,28]. IGBEM was also used for 2D and 3D shape optimizations in [29,30].

A review of IGA was proposed in paper by Nguyen et al. [31] and a review of recent efforts to streamline the CAD-analysis transition pipeline was provided in [32,33]. Note that a wide range of other methods, relying also directly on CAD are also aiming at CAD-analysis integration. One should, in particular, refer to the work of Sevilla et al. [34], Moumnassi et al. [35] and Legrain et al. [36–38]. But significantly complicated adaptive h-refinement since tensor product approximations are still common place. This means that the approximation must be refined everywhere at once in the domain. Alternatives to this were proposed by [22,39], where the geometry and the field approximations are independent. Similar ideas were proposed earlier by Sevilla et al. [34] and allowed to obtain exact boundary representation, as in IGA, but without requiring the interior discretisation to be tied to the geometry representation, offering more flexibility. A second difficulty encountered by IGA is the need for an interior parameterisation to be constructed from the CAD data, which only provides boundary information. Significant work was already performed to achieve this, notably [40] where collocation methods/meshfree approximations are constructed within the domain whilst preserving geometry exactness. Finally, isogeometric boundary element methods [23,24] are probably the best suited candidates to overcome this interior discretisation obstacle, since only boundary data is required for analysis, which enables, for example, stress analysis [23,25], acoustic problems [41], potential problems [42,43] and damage tolerance/crack propagation analysis [27] to be performed without any mesh generation step, directly from CAD.

In this paper, the adaptive integration scheme based on sub-division technique presented in [44] is coupled with the IGBEM to control the numerical error of the integration. Adaptive scheme accounts for nearly singular and singular integrals existing in BEM problems [25,43]. In [45,46], an adaptive scheme was introduced for fracture problems. Cirak et al. proposed in 2000 a method based on subdivision surfaces for thin-shell finite element analysis [47]. In 2002, Cirak et al. [48] also proposed an integrated modeling FEA and engineering design approach for thin-shell structures using subdivision surfaces. This work is concerned with the calculation of the effective thermal conductivity of steady state heterogeneities using an adaptive IGBEM.

The composite considered in this work is assumed to be misoriented in space, namely, statistically homogeneous [49,50]. Following the method in [13], the integral equation formulations which only contain the unknown temperatures on the interface are used in the implementation of the IGBEM. And a heat energy computation formulation which only contains the interface integrals is adopted to calculate the system heat energy. Based on the GSCS model, some numerical examples are solved. The present results are compared with the exact solutions or upper and lower bounds of solutions. The results show the accuracy and effectiveness of the present method.

A short description of the contents of this paper is as follows. Section 2 introduces necessary background concepts about GSCS and the differential formulations of the physical problem. Section 3 presents the formulations for isogeometric GSCS model. Section 4 gives the adaptive integration scheme for boundary integrals on isogeometric element. In Section 5, the computation process of the isogeometric GSCS is described. Several numerical examples are given in Section 6 to verify the efficiency and accuracy of the present method. Finally, we present the conclusions for our work.

2. Problem statement

GSCS takes into account the interaction between matrix and inclusions by considering a representative unit cell inclusion, i.e., an inclusion and a surrounding matrix, which is itself embedded in the infinite effective matrix. Owing to considering the full range of the volume fraction of inclusion, it gives a physically realistic model of inclusion to inclusion interaction for two-phase system. The generalized self-consistent model of the presented problem is shown in Fig. 1, where the geometry of the model is described by NURBS. More details about principles of GSCS model can be found in [5,9–11,13].

As shown in Fig. 1, assume that Γ_1 and Γ_2 represent the inclusion-original matrix interface and the original matrix-effective matrix interface, respectively. The heat fluxes along x, y and z axes are indicated by q_x,q_y and q_z, respectively. Here, we focus our attention on the numerical implementation of the adaptive IGBEM for calculation of effective heat conductivity of steady state heterogeneity. Thus, only some conclusions are given, more details about basic idea and derivation process of boundary integral equation can be found in [13].

According to several boundary integral equations obtained by the location of the source points and continuity condition [13], the following formulas which only contain the unknown temperatures on the interface can be obtained. When the source point P is on Γ_2, we have the following integral equation:

$$\left(c_E(P)+\frac{k_M}{k_E}c_M(P)\right)u_E(P)=u^0(P)-\int_{\Gamma_2}\left(1-\frac{k_M}{k_E}\right)T_E(P,q)u_E(q)d\Gamma - \int_{\Gamma_1}\left(\frac{k_M-k_I}{k_E}\right)T_M(P,q)u_M(q)d\Gamma \quad (1)$$

where k_I, k_M and k_E are the thermal conduction coefficients of the

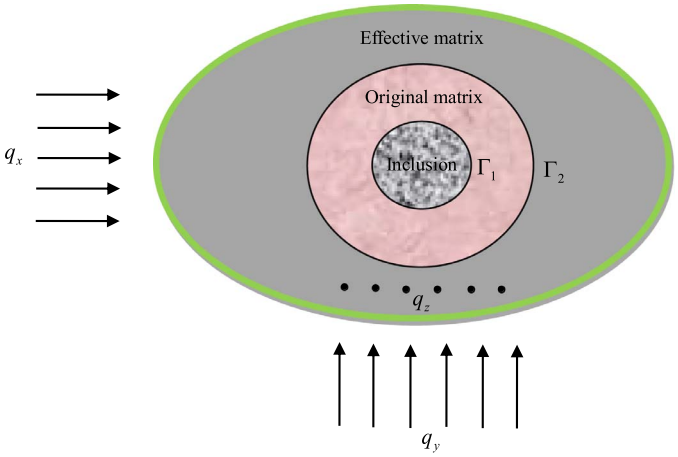

Fig. 1. The GSCS model with single inclusion.

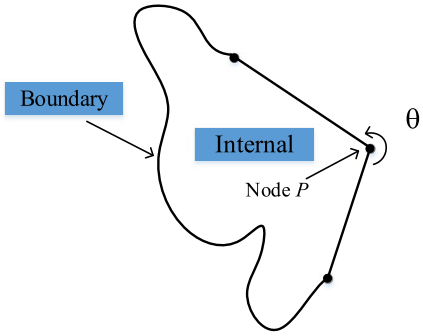

Fig. 2. 2D boundary.

inclusion, original matrix and effective matrix, respectively. c_E and c_M are coefficients to be evaluated at the boundary point. In the case of 2D, it is easy to visualize $c_E(P)$ as the ratio of the external angle θ and 2π [51], i.e. $c_E(P) = 1-\frac{\theta}{2\pi}$, where θ is shown in Fig. 2. $u^0(P)$ is the temperature on the source point P for the whole body composed of the effective material under the far field heat fluxes [52]. u_E and u_M are the temperatures over the interfaces Γ_1 and Γ_2, respectively. The fundamental solutions T_E and T_M for 3D steady state systems [53] are of the following forms:

$$T_E = T_M = \frac{1}{4\pi r^2}\frac{\partial r}{\partial \mathbf{n}} \tag{2}$$

where r is the distance between the source point P and the field point q. $\boldsymbol{n}$ is the outward unit normal on the interface. $(\partial r/\partial \mathbf{n}) = n_i(\partial r/\partial x_i)$ in which Einstein sum convention is adopted throughout the paper.

And when the source point is on Γ_1, the corresponding integral equation can be written as follows:

$$\left(\frac{k_I c_I(P) + k_M c_M(P)}{k_E}\right)u_M(P) = u^0(P) - \int_{\Gamma_2}\left(1-\frac{k_M}{k_E}\right)T_E(P,q)u_E(q)d\Gamma - \int_{\Gamma_1}\left(\frac{k_M-k_I}{k_E}\right)T_M(P,q)u_M(q)d\Gamma \tag{3}$$

Eqs. (1) and (3) which only contain the unknown temperatures u_E and u_M on the interface, can be used to investigate the steady state heterogeneous medium under the various remote thermal loading, i.e. temperature, heat flux and their combinations.

In the GSCS, the effective thermal conductivity k_E is an unknown value which needs to be iteratively solved. Therefore, the derivatives of Eqs. (1) and (3) with respect to the unknown effective thermal conductivity k_E give us the following integral equations:

$$\left(c_E(P)+\frac{k_M}{k_E}c_M(P)\right)\dot{u}_E(P) - \frac{k_M}{k_E^2}c_M(P)u_E(p) = \dot{u}^0(P) - \int_{\Gamma_2}\left(1-\frac{k_M}{k_E}\right)T_E(P,q)\dot{u}_E(q)d\Gamma - \int_{\Gamma_2}\frac{k_M}{k_E^2}T_E(P,q)u_E(q)d\Gamma - \int_{\Gamma_1}\left(\frac{k_M-k_I}{k_E}\right)T_M(P,q)\dot{u}_M(q)d\Gamma + \int_{\Gamma_1}\left(\frac{k_M-k_I}{k_E^2}\right)T_M(P,q)u_M(q)d\Gamma,\ (P\in\Gamma_2) \tag{4}$$

and

$$\begin{aligned}&\left(\frac{k_M c_M(P)+k_I c_I(P)}{k_E}\right)\dot{u}_E(P) - \left(\frac{k_M c_M(P)+k_I c_I(P)}{k_E^2}\right)u_E(P)\\ &= \dot{u}^0(P) - \int_{\Gamma_2}\left(1-\frac{k_M}{k_E}\right)T_E(P,q)\dot{u}_E(q)d\Gamma - \int_{\Gamma_2}\frac{k_M}{k_E^2}T_E(P,q)u_E(q)d\Gamma\\ &\quad - \int_{\Gamma_1}\left(\frac{k_M-k_I}{k_E}\right)T_M(P,q)\dot{u}_M(q)d\Gamma\\ &\quad + \int_{\Gamma_1}\left(\frac{k_M-k_I}{k_E^2}\right)T_M(P,q)u_M(q)d\Gamma,\quad (P\in\Gamma_1)\end{aligned} \tag{5}$$

where the dot above the temperature u denotes derivative with respect to k_E, i.e. $\dot{u} = \partial u/\partial k_E$.

In this section, the basic idea and formulas for the present work are given. For the GSCS model, the u^0 and $\dot{u}^0$ are known quantities which can be obtained by the given heat fluxes q_x, q_y and q_z. The effective thermal conductivity k_E existing in Eqs. (1), (3), (4) and (5) is the unknown quantity. And the detailed calculation process is given in Section 5.

3. Formulations for isogeometric GSCS model

Different from the GSCS model based on conventional BEM, the present GSCS model can exactly capture the geometry due to the basis function of the IGBEM. When the procedure of refinement is acquired for the model, the exact geometry will be maintained at all stages of analysis.

In the implementation of the GSCS, we use two knot vectors $\mathbf{U} = \{\xi_1,\xi_2,\ldots,\ \xi_{n+p+1}\}$ and $\mathbf{V} = \{\eta_1,\eta_2,\ldots,\eta_{m+q+1}\}$, $m \times n$ control points $\{P_{i,j}\}$, $i = 1, 2, \ldots, n$, $j = 1, 2, \ldots, m$, and curve orders p and q to build the interface shapes and the basis functions. As shown in Fig. 3, "elements" of the integral boundary are defined in the parametric space as non-zero knots span $[\xi_i, \xi_{i+1}] \times [\eta_j, \eta_{j+1}]$, where $\xi_i, \xi_{i+1} \in \mathbf{U}$ and $\eta_j, \eta_{j+1} \in \mathbf{V}$.

In order to carry out the numerical integration using Gauss–Legendre quadrature, local coordinates $\bar{\xi}$ and $\bar{\eta}$ must be in the range [-1, 1] × [-1, 1]. Therefore, there should be a transformation from the parameter space $(\xi, \eta) \in [\xi_i, \xi_{i+1}] \times [\eta_j, \eta_{j+1}]$ (ξ_i is the ith knot in $\mathbf{U}$ and η_j is the jth knot in $\mathbf{V}$, i and j are respectively the knot indexes in directions ξ and η) to the Gauss–Legendre range [-1, 1] × [-1, 1]. Fig. 3 gives some illustration for physical domain Ω, parametric domain $\widehat{\Omega}$ and parent element.

The transformation from the physical domain to a parametric domain is given by

$$d\Omega = |J_{(\xi\eta)}|d\xi d\eta \tag{6}$$

where

$$|J_{(\xi\eta)}| = \left[\left(\frac{\partial x_2}{\partial\xi}\frac{\partial x_3}{\partial\eta} - \frac{\partial x_3}{\partial\xi}\frac{\partial x_2}{\partial\eta}\right)^2 + \left(\frac{\partial x_3}{\partial\xi}\frac{\partial x_1}{\partial\eta} - \frac{\partial x_1}{\partial\xi}\frac{\partial x_3}{\partial\eta}\right)^2 + \left(\frac{\partial x_1}{\partial\xi}\frac{\partial x_2}{\partial\eta} - \frac{\partial x_2}{\partial\xi}\frac{\partial x_1}{\partial\eta}\right)^2\right]^{1/2} \tag{7}$$

and the transformation from the parent domain to a parametric domain is given by

$$\begin{aligned}\xi &= \tfrac{1}{2}[(\xi_{i+1}-\xi_i)\bar{\xi} + (\xi_{i+1}+\xi_i)]\\ \eta &= \tfrac{1}{2}[(\eta_{j+1}-\eta_j)\bar{\eta} + (\eta_{j+1}+\eta_j)].\end{aligned} \tag{8}$$

where $\bar{\xi}$ and $\bar{\eta}$ represent intrinsic coordinates at a Gauss point. Therefore, the determinant of the Jacobian of this transformation reads

$$|J_{(\bar{\xi}\bar{\eta})}| = \frac{1}{4}(\xi_{i+1}-\xi_i)(\eta_{j+1}-\eta_j) \tag{9}$$

To approximate the geometry and unknown fields, the non-zero basis functions must be determined for a particular element. After this is done, a set of local basis functions that are related to the global basis functions are given as

$$N_b^e(\bar{\xi},\bar{\eta}) \equiv R_a^{p,q}(\xi(\bar{\xi}),\eta(\bar{\eta})) \tag{10}$$

where the local basis function number b, element number e and global basis function number a are related by $a = \mathrm{conn}(e, b)$, where conn() is a

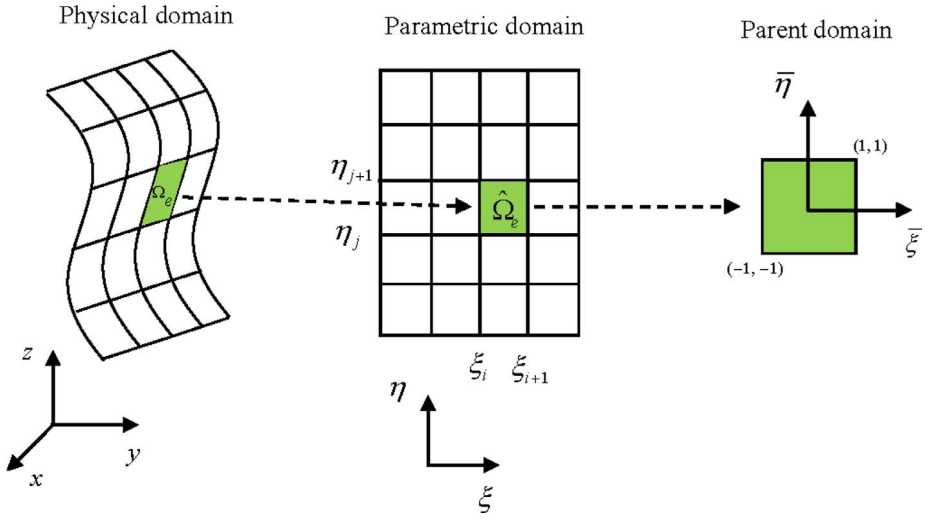

Fig. 3. Definition of domains used for integration in the present method.

connectivity function. As shown in Fig. 4, a 2D example is given to describe the way to build up the connectivity function, where $a = 1, \ldots, 9$, $b = 1,\ldots,3$ and $e = 1,\ldots,4$.

Up to now, the geometry and temperature can be easily interpolated as

$$\mathbf{x}_e(\bar{\xi}, \bar{\eta}) = \sum_{b=1}^{(p+1)(q+1)} N_b^e(\bar{\xi}, \bar{\eta})\mathbf{x}_b$$
$$u_e(\bar{\xi}, \bar{\eta}) = \sum_{b=1}^{(p+1)(q+1)} N_b^e(\bar{\xi}, \bar{\eta})u_b \tag{11}$$

where $\mathbf{x}_b$ and u_b represent the coordinate, temperature coefficients at a particular control point, respectively.

For the purpose of numerical computation, the boundary surface should be discretized into a non-overlapping set of N elements giving

$$\Gamma = \bigcup_{e=1}^{N} \Gamma_e, \quad \Gamma_i \cap \Gamma_j = 0, \quad i \neq j \ (i, j = 1,\cdots,N).$$

Then, Eqs. (1), (3), (4) and (5) can be rewritten:

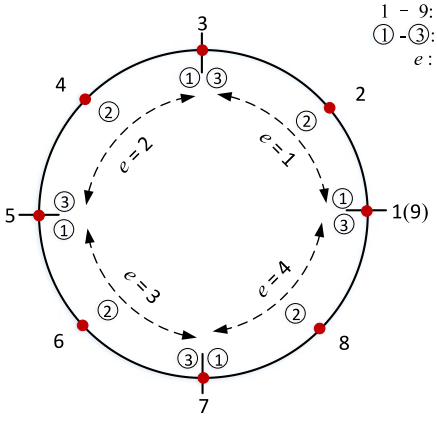

Fig. 4. Illustration of the construction of the connectivity function.

$$\left(c_E(\mathbf{x}') + \frac{k_M}{k_E}c_M(\mathbf{x}')\right)\sum_{l=1}^{(p+1)(q+1)} N_l^{\bar{e}}(\bar{\xi}', \bar{\eta}')u_E^{l\bar{e}}$$
$$= u^0(\mathbf{x}')$$
$$- \sum_{e=1}^{N\Gamma_2}\sum_{l=1}^{(p+1)(q+1)} \int_{-1}^{1}\int_{-1}^{1}\left[\left(1 - \frac{k_M}{k_E}\right)T_E(\mathbf{x}', \mathbf{x}(\bar{\xi}, \bar{\eta}))N_l^e(\bar{\xi}, \bar{\eta})J(\bar{\xi}, \bar{\eta})\right]d\bar{\xi}d\bar{\eta}u_E^{le}$$
$$- \sum_{e=1}^{N\Gamma_1}\sum_{l=1}^{(p+1)(q+1)} \int_{-1}^{1}\int_{-1}^{1}\left[\left(\frac{k_M - k_I}{k_E}\right)T_M(\mathbf{x}', \mathbf{x}(\bar{\xi}, \bar{\eta}))N_l^e(\bar{\xi}, \bar{\eta})J(\bar{\xi}, \bar{\eta})\right]d\bar{\xi}d\bar{\eta}u_M^{le} \tag{12}$$

$$\left(\frac{k_M c_M(\mathbf{x}') + k_I c_I(\mathbf{x}')}{k_E}\right)\sum_{l=1}^{(p+1)(q+1)} N_l^{\bar{e}}(\bar{\xi}', \bar{\eta}')u_M^{l\bar{e}}$$
$$= u^0(\mathbf{x}')$$
$$- \sum_{e=1}^{N\Gamma_2}\sum_{l=1}^{(p+1)(q+1)} \int_{-1}^{1}\int_{-1}^{1}\left[\left(1 - \frac{k_M}{k_E}\right)T_E(\mathbf{x}', \mathbf{x}(\bar{\xi}, \bar{\eta}))N_l^e(\bar{\xi}, \bar{\eta})J(\bar{\xi}, \bar{\eta})\right]d\bar{\xi}d\bar{\eta}u_E^{le}$$
$$- \sum_{e=1}^{N\Gamma_1}\sum_{l=1}^{(p+1)(q+1)} \int_{-1}^{1}\int_{-1}^{1}\left[\left(\frac{k_M - k_I}{k_E}\right)T_M(\mathbf{x}', \mathbf{x}(\bar{\xi}, \bar{\eta}))N_l^e(\bar{\xi}, \bar{\eta})J(\bar{\xi}, \bar{\eta})\right]d\bar{\xi}d\bar{\eta}u_M^{le} \tag{13}$$

$$\left(c_E(\mathbf{x}') + \frac{k_M}{k_E}c_M(\mathbf{x}')\right)\sum_{l=1}^{(p+1)(q+1)} N_l^{\bar{e}}(\bar{\xi}', \bar{\eta}')\dot{u}_E^{l\bar{e}} - \frac{k_M}{k_E^2}c_M(\mathbf{x}')\sum_{l=1}^{(p+1)(q+1)} N_l^{\bar{e}}(\bar{\xi}', \bar{\eta}')u_E^{l\bar{e}}$$
$$= \dot{u}^0(\mathbf{x}')$$
$$- \sum_{e=1}^{N\Gamma_2}\sum_{l=1}^{(p+1)(q+1)} \int_{-1}^{1}\int_{-1}^{1}\left[\left(1 - \frac{k_M}{k_E}\right)T_E(\mathbf{x}', \mathbf{x}(\bar{\xi}, \bar{\eta}))N_l^e(\bar{\xi}, \bar{\eta})J(\bar{\xi}, \bar{\eta})\right]d\bar{\xi}d\bar{\eta}\dot{u}_E^{le}$$
$$- \sum_{e=1}^{N\Gamma_2}\sum_{l=1}^{(p+1)(q+1)} \int_{-1}^{1}\int_{-1}^{1}\left[\frac{k_M}{k_E^2}T_E(\mathbf{x}', \mathbf{x}(\bar{\xi}, \bar{\eta}))N_l^e(\bar{\xi}, \bar{\eta})J(\bar{\xi}, \bar{\eta})\right]d\bar{\xi}d\bar{\eta}u_E^{le}$$
$$- \sum_{e=1}^{N\Gamma_1}\sum_{l=1}^{(p+1)(q+1)} \int_{-1}^{1}\int_{-1}^{1}\left[\left(\frac{k_M - k_I}{k_E}\right)T_M(\mathbf{x}', \mathbf{x}(\bar{\xi}, \bar{\eta}))N_l^e(\bar{\xi}, \bar{\eta})J(\bar{\xi}, \bar{\eta})\right]d\bar{\xi}d\bar{\eta}\dot{u}_M^{le}$$
$$+ \sum_{e=1}^{N\Gamma_1}\sum_{l=1}^{(p+1)(q+1)} \int_{-1}^{1}\int_{-1}^{1}\left[\left(\frac{k_M - k_I}{k_E^2}\right)T_M(\mathbf{x}', \mathbf{x}(\bar{\xi}, \bar{\eta}))N_l^e(\bar{\xi}, \bar{\eta})J(\bar{\xi}, \bar{\eta})\right]d\bar{\xi}d\bar{\eta}u_M^{le} \tag{14}$$

and

$$\left(\frac{k_M c_M(\mathbf{x}') + k_I c_I(\mathbf{x}')}{k_E}\right) \sum_{l=1}^{(p+1)(q+1)} N_l^{\bar{e}}(\bar{\xi}', \bar{\eta}')\dot{u}_E^{l\bar{e}} - \left(\frac{k_M c_M(\mathbf{x}') + k_I c_I(\mathbf{x}')}{k_E^2}\right) \sum_{l=1}^{(p+1)(q+1)} N_l^{\bar{e}}(\bar{\xi}', \bar{\eta}')u_E^{l\bar{e}}$$
$$= \dot{u}^0(\mathbf{x}') - \sum_{e=1}^{N\Gamma_2} \sum_{l=1}^{(p+1)(q+1)} \int_{-1}^{1}\int_{-1}^{1} \left[\left(1 - \frac{k_M}{k_E}\right) T_E(\mathbf{x}', \mathbf{x}(\bar{\xi}, \bar{\eta}))N_l^e(\bar{\xi}, \bar{\eta})J(\bar{\xi}, \bar{\eta})\right] d\bar{\xi}d\bar{\eta}\dot{u}_E^{le}$$
$$- \sum_{e=1}^{N\Gamma_2} \sum_{l=1}^{(p+1)(q+1)} \int_{-1}^{1}\int_{-1}^{1} \left[\frac{k_M}{k_E^2} T_E(\mathbf{x}', \mathbf{x}(\bar{\xi}, \bar{\eta}))N_l^e(\bar{\xi}, \bar{\eta})J(\bar{\xi}, \bar{\eta})\right] d\bar{\xi}d\bar{\eta}u_E^{le}$$
$$- \sum_{e=1}^{N\Gamma_1} \sum_{l=1}^{(p+1)(q+1)} \int_{-1}^{1}\int_{-1}^{1} \left[\left(\frac{k_M - k_I}{k_E}\right) T_M(\mathbf{x}', \mathbf{x}(\bar{\xi}, \bar{\eta}))N_l^e(\bar{\xi}, \bar{\eta})J(\bar{\xi}, \bar{\eta})\right] d\bar{\xi}d\bar{\eta}\dot{u}_M^{le}$$
$$+ \sum_{e=1}^{N\Gamma_1} \sum_{l=1}^{(p+1)(q+1)} \int_{-1}^{1}\int_{-1}^{1} \left[\left(\frac{k_M - k_I}{k_E^2}\right) T_M(\mathbf{x}', \mathbf{x}(\bar{\xi}, \bar{\eta}))N_l^e(\bar{\xi}, \bar{\eta})J(\bar{\xi}, \bar{\eta})\right] d\bar{\xi}d\bar{\eta}u_M^{le} \tag{15}$$

where l is a local node number, on element e, that varies from 1 to $m = 2, 3, \ldots$ for linear, quadratic elements etc. N_l^e is the local shape function for node l. J is the Jacobian of transformation. $\bar{\xi} \in [-1, 1]$ and $\bar{\eta} \in [-1, 1]$ are respectively local coordinates. u^{le} represents temperature at local node l on element e. x' indicates the collocation point and $\bar{\xi}'$ and $\bar{\eta}'$ represent the local coordinates of the collocation point on element $\bar{e}$.

4. Adaptive integration scheme for boundary integrals on isogeometric element

For standard Gauss quadrature the integral of a function $f(x)$ between arbitrary limits (a, b) can be approximated by the weighted sum of a discrete number of function values, normally evaluated at certain sampling points (ordinates) between the two limits. In general, the Gaussian quadrature formula for a surface in three dimensions can be expressed in the intrinsic coordinate system by the equation

$$I = \int_{-1}^{1}\int_{-1}^{1} f(\xi, \eta)d\xi d\eta = \sum_{i=1}^{m_1}\sum_{j=1}^{m_2} w_1^i w_2^j f(\xi^i, \eta^j) + E_1 + E_2 \tag{16}$$

where ξ^i,η^j are the Gauss ordinates, w_1^i, w_2^j are the weights, m_1,m_2 are the Gauss orders, and E_1,E_2 are the integration errors in the two directions. In 1984, Mustoe [54] proposed the following approximate formula for the upper bound of the relative error $e_i = E_i/I$ in the ith direction.

$$e_i \le 2\left(\frac{L_i}{4R}\right)^{2m_i} \frac{(2m_i + \beta - 1)!}{(2m_i)!(\beta - 1)!} \tag{17}$$

where $\beta > 1$ is the order of singularity of the integrand $r^{-\beta}$, L_i is the length of the element in the ith direction, and R is the minimum distance from the source point to the element, as shown in Fig. 5.

In order to avoid using excessively high Gauss order m_i, the elements should be further divided into sub-elements to reduce the L_i/R ratio. It should be pointed out that, for this method, the nearly singular integrals can be accurately computed by using normal Gauss orders when the ratio L_i/R will not be too large.

Based on [44,55,56], Eq. (17) can be approximated by the expression

$$m_i = \sqrt{\frac{2}{3}\beta + \frac{2}{5}}\,[-0.1\ln(e_i/2)][(8L_i/3R)^{3/4} + 1] \tag{18}$$

which can be rearranged to yield:

$$L_i = \frac{3}{8}R\left(\frac{-10m_i}{\sqrt{2\beta/3 + 2/5}\ln(e_i/2)} - 1\right)^{4/3} \tag{19}$$

where e_i is the given relative error and $e_i = 10^{-9}$. Using this approximation, the required Gauss order is obtained explicitly, rather than through iteration. Alternatively, given a maximal Gauss order, the corresponding sub-element dimensions can be obtained explicitly. Now, in order to implement an adaptive integration scheme based on these criteria, it is necessary to devise efficient methods for determining the geometric parameters R and L for each collocation point and for each element, or sub-element. Details of derivation and implementation can be found in [44,56].

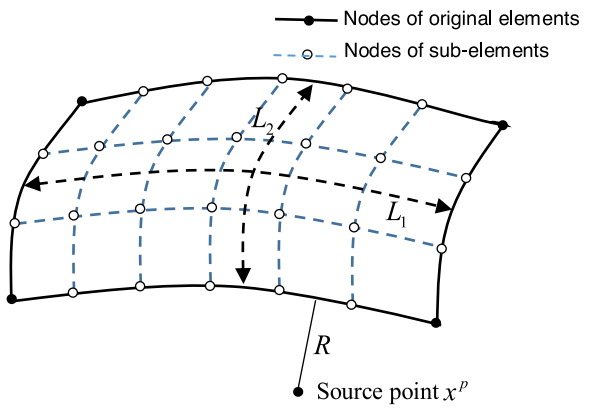

Fig. 5. Element sub-division technique.

4.1. Calculation of sub-element length

In any isogeometric element, Cartesian coordinates can be determined from the control points, i.e.

$$\mathbf{x}_e(\xi, \eta) = \sum_{b=1}^{(p+1)(q+1)} N_b^e(\xi, \eta)\mathbf{x}_b \tag{20}$$

where $\mathbf{x}_b$ represents the coordinates at a particular control point.

In this paper, the length of a boundary element, in the ith intrinsic direction ($[\xi_l,\xi_{l+1}]$or $[\eta_l,\eta_{l+1}]$) is defined by the length of the curve through the center of the element along the integration direction (as shown in Fig. 5). For three dimension case, the length of a boundary element can be accurately calculated using

$$L_i = \int_{\xi_l}^{\xi_{l+1}} \sqrt{\sum_{j=1}^{3}\left(\frac{\partial x_j}{\partial \xi_i}\right)^2} d\xi_i = \int_{-1}^{1} \sqrt{\sum_{j=1}^{3}\left(\sum_{b=1}^{(p+1)(q+1)} \frac{\partial N_b^e}{\partial \xi_i} x_b\right)^2} \frac{\xi_{l+1} - \xi_l}{2} d\xi_i \tag{21}$$

4.2. Calculation of minimum distance r

To determine the minimum distance R from source point to an element, Gao and Davies [44,56] proposed a Newton–Raphson iterative scheme for traditional BEM. Here, the method is also used to the IGBEM.

First, we begin with some starting guess (ξ_0) of the intrinsic coordinates of the source point and we let r_j^0 be the resulting error in the computation of the jth component of the global coordinates of the source point. Now, the notation r_j^k is used to denote the value after the kth iteration in the Newton–Raphson iterative scheme, that is:

$$r_j^k = \sum_{b=1}^{(p+1)(q+1)} N_b^e\, x_j^b - x_j \tag{22}$$

where x_j is the jth component of the global coordinates of the source point and x_j^b represents the jth component at a particular control point.

To obtain improved values of ξ_i, we expand this equation using Taylor's theorem:

$$r_j^{k+1} = r_j^k + \frac{\partial r_j}{\partial \xi_i}\Delta\xi_i = r_j^k + \sum_{b=1}^{(p+1)(q+1)} \frac{\partial N_b^e}{\partial \xi_i} x_j^b \Delta\xi_i \tag{23}$$

Step 1. Compute the elements of the integral boundary which are defined in the parametric space as non-zero knots span $[\xi_i, \xi_{i+1}]\times[\eta_j, \eta_{j+1}]$.

Step 2. Calculate element length L_i and minimum distance R from the source point in integral equation to elements.

Step 3. Calculate the Gauss order m_i with specified precision.

Step 4. If $m_i \le m_{\max}$, using Gaussian quadrature evaluates the integral.

Step 5. if $m_i > m_{\max}$, using $m_i = m_{\max}$ calculate the permitted maximum length $L_i^{\max}$.

Step 6. Divide element into equal sub-elements. And calculate the length of each sub-element L_i^s.

Step 7. Calculate the minimum distance R_n from the source point to the nth sub-element.

Step 8. Calculate the Gauss order m_i^n for the nth sub-element.

Step 9. Apply Gauss quadrature formulae to evaluate the integral over the sub-element.

Step 10. Repeat **Step** 7- 9 for all sub-elements.

Fig. 6. The adaptive integration scheme for the present method.

Step 1. Build the isogeometric GSCS model of matrix and inclusions using CAD software.

Step 2. Read the parameters of material, i.e. temperature, heat flux (q_x, q_y, q_z) and the thermal conductivity of matrix and inclusion k_M, k_I.

Step 3. Initialize effective thermal conductivity k_e which can be assumed to be k_M.

Step 4. Calculate solution $\mathbf{u}$ of Eq. (29).

Step 5. Calculate the left hand side of Eq. (33), i.e.

$$f(k_E) = \left\{(k_{jM} - k_{jI})\int_{\Gamma_{j1}} n_i q_i^0 u d\Gamma + (k_E - k_{jM})\int_{\Gamma_{j2}} n_i q_i^0 u d\Gamma\right\}$$

Step 6. If $f(k_E)$ is less than the given tolerance, then to store k_M as the final effective thermal conductivity and to stop iteration.

Step 7. Otherwise, calculate temperature derivative $\dot{\mathbf{u}}$ using Eq. (30).

Step 8. Calculate $\Delta k_E = -f(k_M)/\dot{f}(k_M)$ in which

$$\dot{f}(k_E) = \left\{(k_{jM} - k_{jI})\int_{\Gamma_{j1}} n_i q_i^0 \dot{u} d\Gamma + (k_E - k_{jM})\int_{\Gamma_{j2}} n_i q_i^0 \dot{u} d\Gamma + \int_{\Gamma_{j2}} n_i q_i^0 u d\Gamma\right\}$$

Step 9. Calculate $k_E = k_E + \Delta k_E$

Step 10. Go to **Step** 4.

Fig. 7. The process of the isogeometric GSCS.

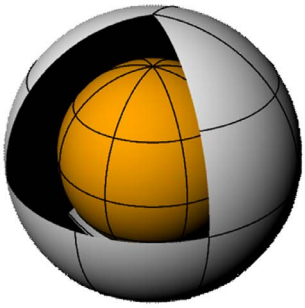

(a) Spherical inclusion and spherical matrix.

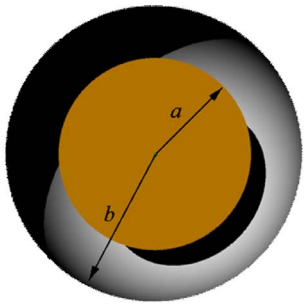

(b) Cross-section cut by *xz* plane.

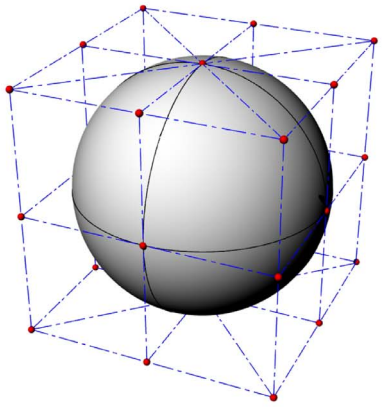

(c) The control points of the model.

Fig. 8. Isogeometric GSCS spherical model.

Table 1
Polynomial orders and knot vectors for both the matrix and inclusion.

Direction	Order	Knot vector
ξ	$p = 2$	**U** = {0, 0, 0, 1, 1, 2, 2, 3, 3, 4, 4, 4}
η	$q = 2$	**V** = {0, 0, 0, 1, 1, 2, 2, 3, 3, 4, 4, 4}

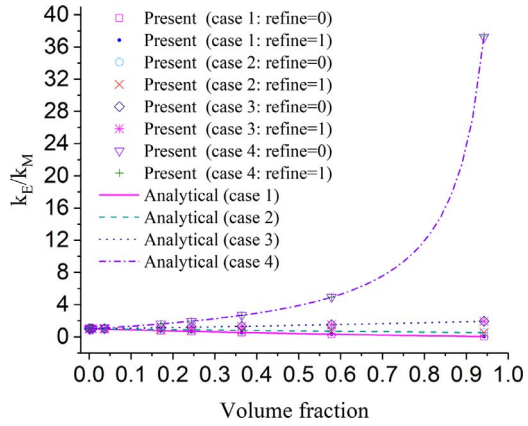

Fig. 9. Varieties of effective thermal conductivity with inclusion volume fraction for isogeometric GSCS spheroidal model (case 1: $k_I/k_M = 0$; case 2: $k_I/k_M = 0.5$; case 3: $k_I/k_M = 2$; case 4: $k_I/k_M = 150$).

where $\Delta\xi_i$ is the change in ξ_i. Setting $r_j^{k+1} = 0$, we can obtain using the Newton–Raphson iterative scheme:

$$[K^k]\{\Delta\xi\} = -\{r^k\} \tag{24}$$

where the coefficients of the matrix are:

$$[K_{ij}^K] = \sum_{b=1}^{(p+1)(q+1)} \frac{\partial N_b^e}{\partial \xi_i} x_j^b$$

Unless the calculations are being carried out for a volume cell, there will be one less intrinsic coordinate than global coordinate. Hence Eq. (24) is over-prescribed. In that case, the least-squares approximation will suffice, i.e.

$$[K^k]^{\mathrm{T}}[K^k]\{\Delta\xi\} = -[K^k]^{\mathrm{T}}\{r^k\} \tag{25}$$

where the superscript T denotes the matrix transpose. Solving for $\{\Delta\xi\}$, the current value of ξ_i can be updated, thus

$$\xi_i^{k+1} = \xi_i^k + \Delta\xi_i \tag{26}$$

We now make the assumption that the proximal point has the intrinsic coordinates defined by the following equations:

$$\begin{aligned} &\xi_i = \xi_i^{k+1}, \quad (\text{if } \xi_i \le |\xi_i^{k+1}| \le \xi_{i+1}) \\ &\xi_i = \xi_i, \quad (\text{if } |\xi_i^{k+1}| \le \xi_i) \\ &\xi_i = \xi_{i+1}, \quad (\text{if } |\xi_i^{k+1}| \ge \xi_{i+1}) \end{aligned} \tag{27}$$

The minimum distance can then be calculated by the following formula:

$$R = \sqrt{\sum_{j=1}^{3} R_j^2} \tag{28}$$

where R_j is the jth Cartesian component of the minimum distance and is determined from the intrinsic coordinates of the proximal point.

Table 2
Values of Δk_E for different cycles, run time, numerical results obtained by the present method and exact results for varying values of α.

α	Δk_E							k_E		Run time
	1st	2nd	3rd	4th	5th	6th	7th	Present	Exact	
$1/(1.08)^3$	1.67E-05	4.34E-06	1.13E-06	2.93E-07	7.63E-08	1.98E-08	5.16E-09	0.58897	0.58896	35″499
$1/(1.4)^3$	6.27E-05	6.32E-06	6.38E-07	6.43E-08	6.49E-09			0.79625	0.79620	14″679
$1/(2.0)^3$	2.87E-05	9.28E-07	3.01E-08	9.74E-10				0.92686	0.92683	7″949
$1/(2.6)^3$	1.33E-05	1.93E-07	2.79E-09	4.05E-11				0.96626	0.96625	5″534
$1/(3.2)^3$	7.12E-06	5.51E-08	4.26E-10					0.98181	0.98180	4″63
$1/(3.8)^3$	4.25E-06	1.95E-08	9.00E-11					0.98911	0.98911	4″39
$1/(4.4)^3$	2.73E-06	8.09E-09	2.40E-11					0.99298	0.99297	4″397
$1/(5.0)^3$	1.86E-06	3.75E-09	7.56E-12					0.99521	0.99521	4″96

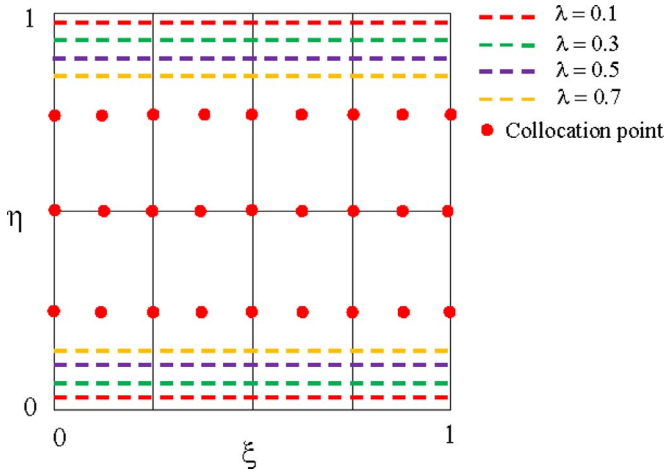

Fig. 10. Parametric space for collocation points that lie at the top and bottom poles moving to dashed places.

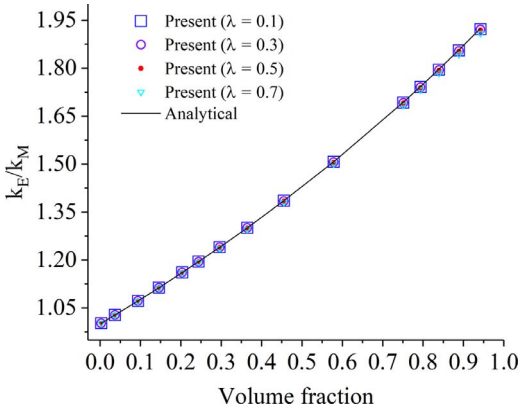

Fig. 11. Varieties of effective thermal conductivity with inclusion volume fraction when λ = 0.1, 0.3, 0.5 or 0.7.

4.3. Adaptive integration scheme

The adaptive integration scheme employs the element sub-division technique described above. In [44,56], the authors have used the scheme to conventional boundary element method. Here, we will expand the method to 3D IGBEM. The implementation process is summarized in Fig. 6.

5. The process of the isogeometric GSCS

For the isogeometric element $([\xi_i, \xi_{i+1}] \times [\eta_j, \eta_{j+1}]$, shown in Fig. 3) used in this paper, 9 collocation points are collocated at the element. And the geometry of the element is described by NURBS basis functions. Here, we used the Greville abscissae definition [23,24] to define the position of collocation points in parameter space. In [42,43], the method has been used to produce collocation points for 3D problems.

In calculation, isogeometric element $([\xi_i, \xi_{i+1}] \times [\eta_j, \eta_{j+1}]$, shown

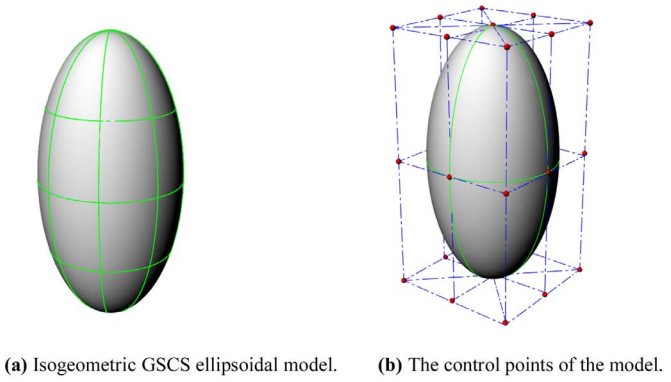

(a) Isogeometric GSCS ellipsoidal model. **(b)** The control points of the model.

(c) Cross-section cut by *xz* plane. **(d)** Cross-section cut *yz* plane.

Fig. 12. Isogeometric GSCS ellipsoidal model.

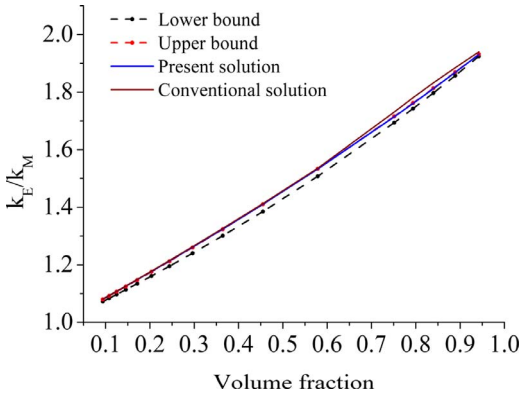

Fig. 13. Varieties of effective thermal conductivity with inclusion volume fraction when $k_I = 2$.

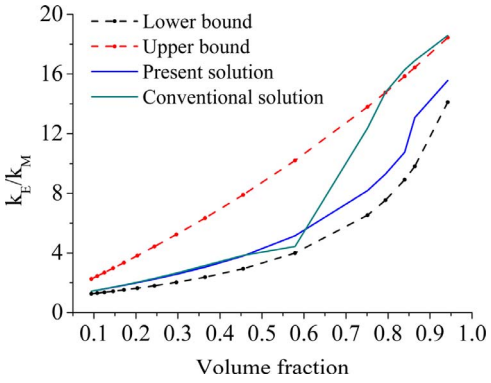

Fig. 14. Varieties of effective thermal conductivity with inclusion volume fraction when $k_I = 20$.

in Fig. 3) is used to discretize the above integral Eqs. (12)–(15) for the analysis. Accordingly, the corresponding matrix equations can be obtained:

$$\mathbf{Hu} = \mathbf{u}^0 \tag{29}$$

and

$$H\dot{\mathbf{u}} = \dot{\mathbf{u}}^0 - \dot{\mathbf{H}}u \tag{30}$$

where $\mathbf{u}$ and $\mathbf{u}^0$ are the unknown and known nodal values of the temperature u, respectively. $\dot{\mathbf{u}}$ and $\dot{\mathbf{u}}^0$ are the corresponding derivatives with respect to the effective thermal conductivity. $\mathbf{H}$ and $\dot{\mathbf{H}}$ are the related coefficient matrix from Eqs. (14) and (15). Once the interface temperature is obtained using Eq. (29), the heat energy of the steady state thermal conduction problem can be computed using the following equation [57]:

$$E = E^0 + \frac{1}{2k_E}\left\{(k_{jM} - k_{jI})\int_{\Gamma_{j1}} n_i q_i^0 u d\Gamma + (k_E - k_{jM})\int_{\Gamma_{j2}} n_i q_i^0 u d\Gamma\right\} \tag{31}$$

where $E^0 = \frac{1}{2}\int_V q_i^0 T_{,i}^0 dV$ which is the heat energy in the homogeneous medium composed of the effective material. The superscript 0 denotes those values from the homogeneous medium subject to remote heat loadings.

The generalized self-consistent scheme demands the following condition [58]:

$$E = E^0 \tag{32}$$

Thus, using Eqs. (32) and (31) becomes

$$\frac{1}{2k_E}\left\{(k_{jM} - k_{jI})\int_{\Gamma_{j1}} n_i q_i^0 u d\Gamma + (k_E - k_{jM})\int_{\Gamma_{j2}} n_i q_i^0 u d\Gamma\right\} = 0 \tag{33}$$

Iterative method for Eqs. (29), (30) and (33) is used to obtain the effective thermal conductivity of the studied problem.

The computational process is shown in Fig. 7, i.e.

As is well-known when the collocation point belongs to the computed element and the corresponding integral is defined as a Cauchy Principal Value (CPV) integral which plays a key role in the implementation of any such method. In this work, CPV integral is calculated by the power series expansion method [59]. In [42,43], the method was used to compute the CPV integrals appearing in the 3D isogeometric boundary element method and detailed computational process was given.

6. Numerical examples

6.1. Concentric spherical GSCS model

As shown in Fig. 8(a) and (b), the problem consists of a spherical inclusion with radius a enclosed by a spherical matrix with radius b embedded in an effective thermal conduction matrix subject to remote heat flux q_0. To describe this model, the corresponding polynomial orders and knot vectors are given in Table 1. In this paper, same polynomials and knot vectors are used for both matrix and inclusion. The control points of the isogeometric model are shown in Fig. 8(c). The volume fraction of the inclusion is taken as $\alpha = a^3/b^3$. The thermal conduction coefficients of the inclusion and the matrix are expressed as k_I and k_M, respectively. In numerical implementation, $a = 1$, $k_M = 1$ and $q_0 = 1$ in z direction, four values of k_I are chosen as 0, 0.5, 2 and 150, respectively. All units are assumed to be consistent.

This problem was defined by quadratic NURBS surface for two interfaces of the inclusion-matrix and the matrix-effective matrix, respectively. The analytical solution for this problem has been presented in [60], i.e.

$$k_E = k_M\left(1 + \frac{3v_I}{v_M + 3k_M/(k_I - k_M)}\right) \tag{34}$$

where v_I and v_M are the volume fraction of inclusion and matrix,

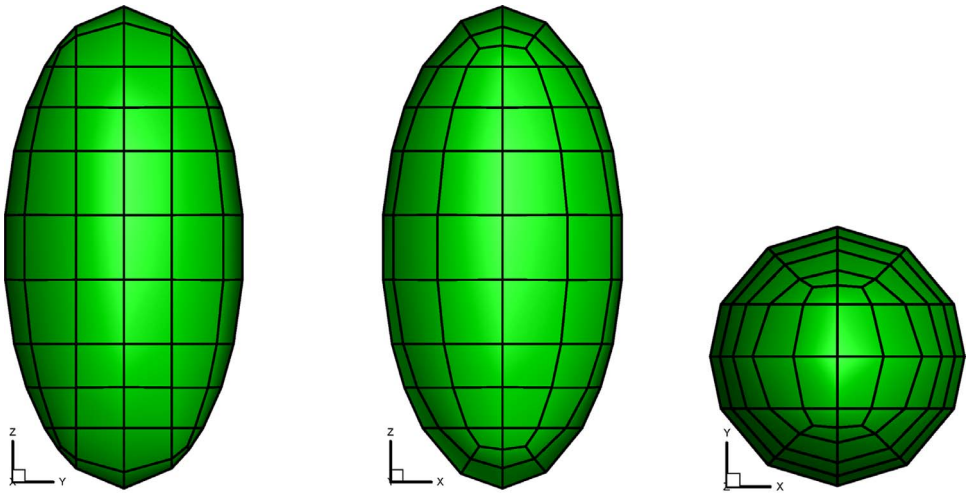

Fig. 15. Mesh of the computed model for the method in [13].

Table 3
Comparisons between the present method and the BEM presented in [13] for varying values of α.

α	Cycle number		Run time		Results			
	Present	BEM [13]	Present	BEM [13]	Lower bound	Present	BEM [13]	Upper bound
$1/(1.04)^3$	13	6	3′ 44″ 93	34″ 951	2.2633749	2.288018	2.358702	2.2974881
$1/(1.08)^3$	13	7	2′ 4″ 116	32″ 267	2.0794722	2.118073	2.236495	2.1323831
$1/(1.20)^3$	12	7	1′21″213	26″ 960	1.7170172	1.768705	1.954430	1.7853403
$1/(1.40)^3$	10	8	1′ 0″ 166	31″ 509	1.4148230	1.460697	1.659448	1.4716981
$1/(1.60)^3$	9	9	49″ 599	30″ 188	1.2657690	1.301500	1.481759	1.3080082
$1/(1.80)^3$	8	9	42″ 502	29″ 233	1.1818623	1.209134	1.366138	1.2130682
$1/(2.00)^3$	8	8	39″ 386	29″ 378	1.1304348	1.151359	1.286496	1.1538462
$1/(2.20)^3$	7	8	35″ 645	29″ 352	1.0969493	1.113207	1.229281	1.1148545
$1/(2.40)^3$	7	8	33″ 382	28″ 40	1.0741253	1.086941	1.186761	1.0880799
$1/(2.80)^3$	6	7	28″ 295	25″ 552	1.0462563	1.054562	1.129030	1.0551673
$1/(3.20)^3$	6	6	28″ 993	21″ 957	1.0308312	1.036486	1.092812	1.0368460
$1/(3.60)^3$	5	5	24″ 672	20″ 999	1.0215877	1.025599	1.068860	1.0258309
$1/(4.00)^3$	5	5	24″ 485	19″ 497	1.0157068	1.018649	1.052340	1.0188088

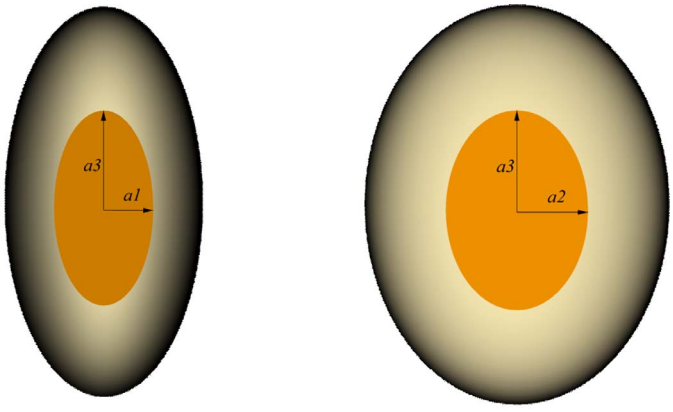

(a) Cross-section cut by *xz* plane. **(b)** Cross-section cut by *yz* plane.

Fig. 16. The cross-sections of isogeometric GSCS ellipsoidal model ($a_1 \neq a_2 < a_3$).

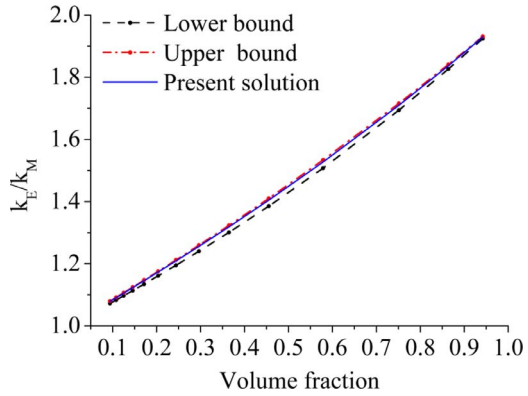

Fig. 17. Varieties of effective thermal conductivity with inclusion volume fraction when $k_I = 2$.

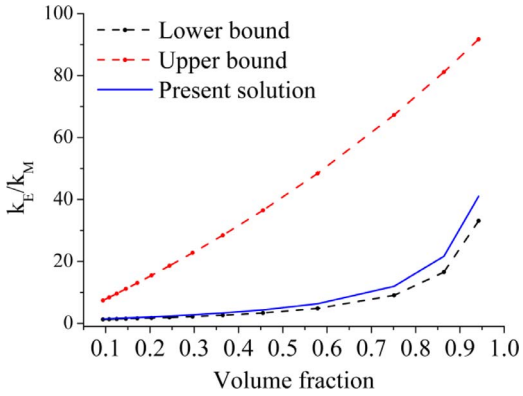

Fig. 18. Varieties of effective thermal conductivity with inclusion volume fraction when $k_I = 100$.

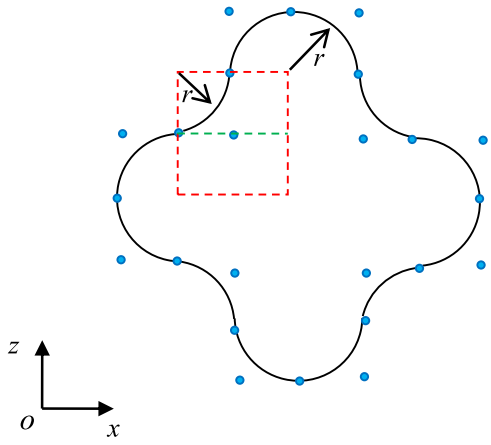

Fig. 19. Meridional cross-section.

respectively.

In this example, *h*-refinement scheme presented in [15] is used to obtain accurate results. As shown in [15], the mechanism for implementing *h*-refinement is knot insertion. Knots may be inserted without changing a curve geometrically or parametrically. Given a knot vector $\mathbf{U} = \{\xi_1,\xi_2,\ldots, \xi_{n+p+1}\}$, let $\overline{\mathbf{U}} = \{\bar{\xi}_1 = \xi_1, \bar{\xi}_2,\ldots,\bar{\xi}_{n+s+p+1} = \xi_{n+p+1}\}$ be an extended knot vector such that $\mathbf{U} \subset \overline{\mathbf{U}}$. Then the new knot vector $\overline{\mathbf{U}}$, which can produce a finer mesh, will be applied to the computation. Here, refine = 0 indicates the original surface corresponding to initial control points and refine = 1 represents the refined surfaces corresponding to more control points. The present results are compared with the analytical solutions as shown in Fig. 9. It can be observed that the present results are in excellent agreement with the analytical solutions. The convergence studies for this problem are performed in both Fig. 9 and Table 2. From Fig. 9, we can observe that the results keep stable

Table 4
Polynomial orders and knot vectors for both the matrix and inclusion.

Direction	Order	Knot vector
ξ	$p = 2$	**U** = {0, 0, 0, 1, 1, 2, 2, 3, 3, 4, 4, 4}
η	$q = 2$	**V** = {0, 0, 0, 1, 1, 2, 2, 3, 3, 4, 4, 5, 5, 6, 6, 6}

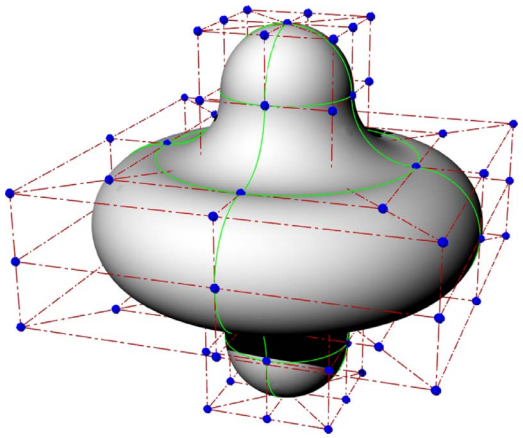

Fig. 20. Isogeometric GSCS complex model.

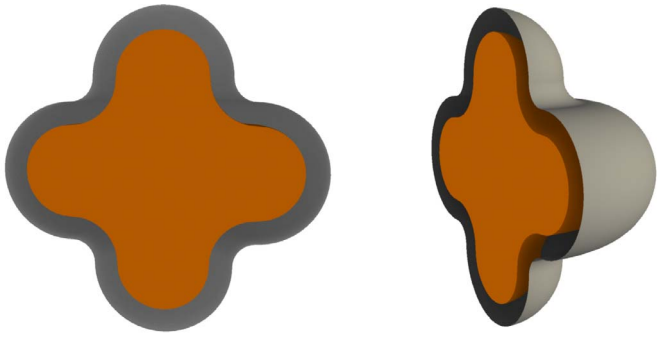

(a) Cross-section cut by *xz* plane. (b) Cross-section cut by the plane *x*=*y*.

Fig. 21. The cross-sections of isogeometric GSCS model.

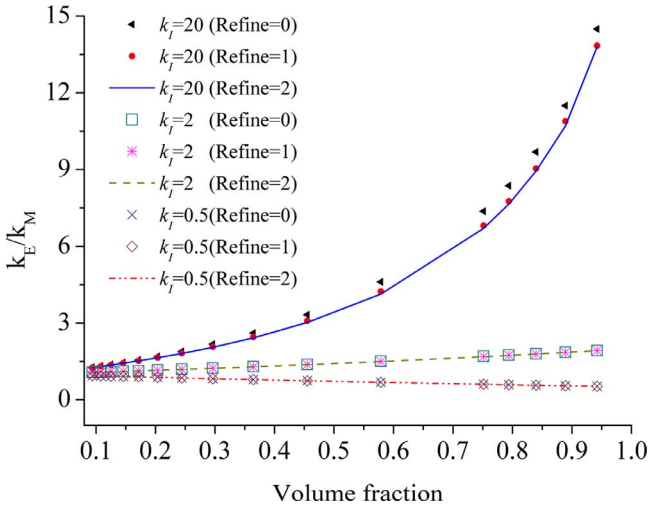

Fig. 22. Varieties of effective thermal conductivity with inclusion volume fraction when k_I=0.5, 2 and 20.

when the mesh is refined.

To give a clear convergence studies for the algorithm shown in Fig. 7, the values of Δk_E for different cycles (steps 4–10 shown in Fig. 7), run time, numerical results obtained by the present method and exact results are given in Table 2. From Table 2, we can see that with the increase of volume fraction of the inclusion (α), more computation time and cycle number are needed due to the adaptive integral method being adopted to compute the nearly singular integrals. When $\alpha < 1/(3.2)^3$, both the computation time and cycle number almost keep stable.

Here, a study about the influence of collocation point locations is given for k_I= 2. For the degenerated elements (shown in Fig. 8), collocation points that lie at the top and bottom poles of the sphere are shifted by Eq. (35) to satisfy the smoothness requirement [41,45]. And the BIEs from these moved collocation points are merged into one equation. As shown in Fig. 10, the collocation points that lie at the top and bottom poles are moved to dashed places which are determined by the values of λ. From Fig. 11, we can see that location of the moved collocation points has little influence on the results of present method.

$$\eta_i = \eta_i + \lambda(\eta_{i+1} - \eta_i), \text{ or}$$
$$\eta_i = \eta_i - \lambda(\eta_i - \eta_{i-1}) \tag{35}$$

where $0 < \lambda < 1$ and η_{i-1}, η_i, $\eta_{i+1} \in \mathbf{V}$, η_i is the parametric of collocation point that lies at the top or bottom pole of the sphere.

6.2. Isogeometric GSCS confocal ellipsoidal model

As shown in Fig. 12, this example studies the problem of an ellipsoidal inclusion with semiaxes a_1,a_2 and a_3 ($a_1 = a_2 < a_3$) enclosed by an ellipsoidal matrix with semiaxes b_1,b_2 and b_3 ($b_1 = b_2 < b_3$) embedded in an effective thermal conduction matrix subject to remote heat flux q_0. The corresponding polynomial orders and knot vectors for this model are the same as that in Table 1 and the control points are given in Fig. 12(b). The volume fraction of the inclusion is taken as $\alpha = a_1a_2a_3/(b_1b_2b_3)$. Similar to the above example, the thermal conduction coefficients of the inclusion and the matrix are expressed as k_I and k_M, respectively. In numerical calculation, $a_1 = 10, a_2 = 10, a_3 = 20$, $b_i = \beta a_i$ (i = 1,2,3; β depends on the volume fraction of the inclusion α), $k_M = 1$ and $q_0 = 1$ in z direction, two values of k_I are chosen as 2 and 20, respectively.

This problem was solved using two different methods, i.e. present IGBEM (present solution) and conventional IGBEM (the IGBEM using the standard Gauss quadrature rather than the adaptive integral method; conventional solution). The results from two methods are shown in Figs. 13 and 14. To illustrate the effectiveness of the results, the following bounds presented by Hashin [61,62] for the effective thermal conductivity of a two-phase composite are also given in Figs. 13 and 14.

$$v_I k_I + v_M k_M - \frac{(k_I - k_M)^2 v_I v_M}{v_I k_M + v_M k_I + 2k_{\min}} \le k_{\text{eff}} \le v_I k_I + v_M k_M - \frac{(k_I - k_M)^2 v_I v_M}{v_I k_M + v_M k_I + 2k_{\max}} \tag{36}$$

where $k_{\max} = \max(k_I, k_M)$, $k_{\min} = \min(k_I, k_M)$, v_I and v_M ($v_I + v_M = 1$) are the volume fractions of inclusion and matrix, respectively.

It follows from Figs. 13 and 14 that when the volume fraction of inclusion is not too big, both the conventional method and the present method are efficient and can yield reasonable results. However, with the increase of the volume fraction, the conventional method performs less satisfactorily which is caused by the nearly singular integral. In contrast, the present method can obtain more reasonable solutions by improving the accuracy of the numerical evaluation of the nearly singular integral.

To examine the superior characteristics of the proposed method, the present method is compared with the boundary element method presented in [13] for k_I=2.5 when the values of α decrease from $1/(1.04)^3$ to $1/(4.00)^3$. For the method in [13], the problem is solved using 124 8-node quadrilateral elements with 374 nodes for two interfaces of the inclusion - matrix and the matrix - effective matrix, respectively (See Fig. 15). The cycle number, run time and results for the two methods are listed in Table 3. The upper and lower bounds of the solution presented in [61,62] are also given in Table 3, from which it can be seen that the results obtained by the method in [13] are a little bigger than the upper bound of the solution. The reason of this phenomenon is that no special method is adopted to deal with the nearly singular integrals and geometrical errors caused by inaccurate geometric approximation

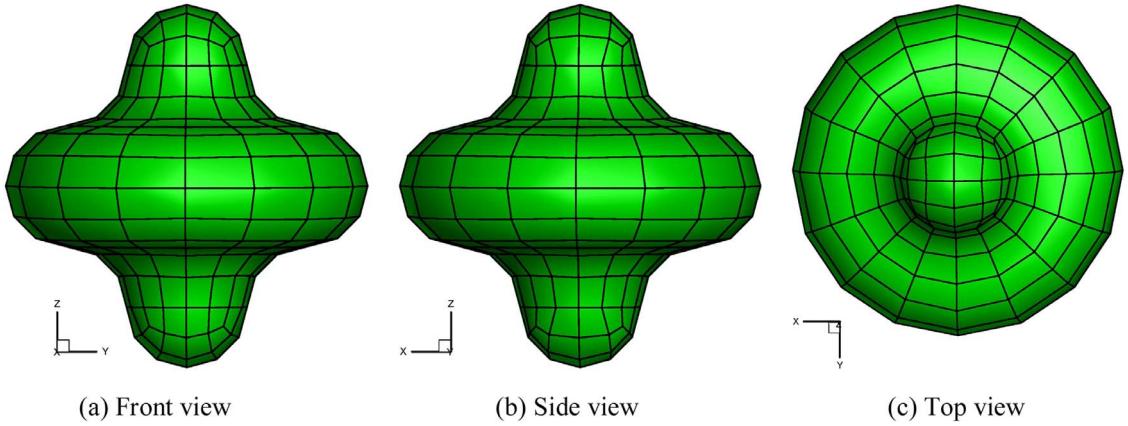

Fig. 23. Mesh of the computed model for the method in [13].

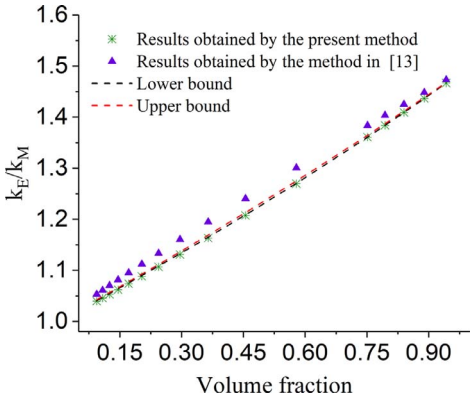

Fig. 24. Varieties of effective thermal conductivity with inclusion volume fraction when $k_I = 1.5$ for two methods.

are produced in the analysis process. However, the present results are located between the upper and lower bounds of the solution even when the volume fraction of the inclusion α is very big. Owing to the adaptive integral method which is used to dealing with the nearly singular integrals, more cycle number and run time are needed in the present method when α is becoming bigger and bigger. And with the decrease of α, the needed cycle number and run time are reduced for the present method.

Furthermore, as shown in Fig. 16, another ellipsoidal inclusion with semiaxes a_1,a_2 and a_3 ($a_1 \neq a_2 < a_3$) enclosed by an ellipsoidal matrix with semiaxes b_1,b_2 and b_3 ($b_1 \neq b_2 < b_3$) embedded in an effective thermal conduction matrix is considered. The present and upper and lower bounds of the solution for $k_I = 2$ and $k_I = 100$ are given in Figs. 17 and 18, respectively. It can be seen from the two figures that the present model can yield a reasonable prediction to the effective thermal conductivity.

6.3. Isogeometric GSCS complex model

The meridional cross-section of the problem is shown in Fig. 19 in which geometrical information is contained. The complex model in this example is obtained by the meridional cross-section rotating 180 along z-axis. To describe this model the corresponding polynomial order and knot vectors are given in Table 4. The 90 initial control points of the model are shown in Fig. 20. This model is embedded in an effective thermal conduction matrix subject to remote heat flux $q_z = q_0$. Fig. 21(a) and (b) give the cross-sections of the isogeometric GSCS model. The area of the cross-section in Fig. 19 can be computed by $4\cdot(4r^2 + \pi r^2/4)$, i.e., a multiple of r^2. Therefore, the volume fraction of the inclusion is taken as α^3 when αr is the radius of each circular arc for inclusion, α is the scaled coefficient of the radius. The thermal conduction coefficients of the inclusion and the matrix are also expressed as k_I and $k_M = 1$, respectively.

Here, refine = 0 also indicates the original surface corresponding to initial control points and refine = 1 or 2 represents the refined surfaces corresponding to more control points, i.e. 370 and 1506, respectively.

The present results with $k_I = 0.5$, $k_I = 2$ and $k_I = 20$ are given in Fig. 22. It can be seen that the results are stable when we refine the mesh for $k_I = 0.5$ and $k_I = 2$. However, with the increase of k_I, a finer mesh should be constructed. The results will be stable when refine = 2 for the complex model with $k_I = 20$.

In this example, the present method is also compared with the method presented in [13] when $k_I = 1.5$. For the method in [13], the problem is solved using 256 8-node quadrilateral elements with 770 nodes for two interfaces of the inclusion - matrix and the matrix - effective matrix, respectively (see Fig. 23). The results of k_E/k_M obtained by the two methods and the upper and lower bounds of the solutions are given in Fig. 24. From Fig. 24, it can be seen that the current results are in good agreement with the upper and lower bounds of the solutions, even for the volume fraction of the inclusion α being very close to 1.0. In contrast, since the existing of geometrical errors, the results obtained by the method in [13] are a little bigger than the upper bounds of the solutions.

7. Conclusions

Based on the GSCS, this work presented an adaptive IGBEM for the calculation of the effective thermal conductivity of steady state heterogeneities. The proposed method has several advantages in comparison with the conventional methods. By adopting the integral equation formulations which only contain the unknown temperatures on the interface, the numerical implementation of the current method become simple and clear. The boundary integrations are calculated easily and effectively at optimal computational cost by introducing the adaptive integral method. Then, the nearly singular integrals appearing in the BEM when the volume ratio of inclusions is getting bigger and bigger can also be computed precisely by the present method. Numerical examples show that the effective thermal conductivity can be effectively obtained by the present method.

Moreover, the geometry data in the present isogeometric GSCS model can be taken directly from CAD programs. The models for analysis are exact geometrical representation no matter how coarse the discretization of the studied bodies are so that no geometrical errors exist in the analysis process. These features can lead to the additional advantages: some practical problems with complex geometry shapes can be easily handled and more accurate effective thermal conductivities can be given. Besides, the meshing process is no longer required because the control points defining the body play the role of

nodes in the isogeometric GSCS.

The method presented can be further used to investigate the shape optimization of steady state thermal conduction problems in the future.

Acknowledgments

The research is supported by the National Natural Science Foundation of China (11672038, 11272054).

References

[1] Rodin G, Weng GJ. On reflected interactions in elastic solids containing inhomogeneities. J Mech Phys Solids 2014;68:197–206.
[2] Norris AN. A differential scheme for the effective moduli of composites. Mech Mater 1985;4(1):1–16.
[3] Chen Y, Balan K, Agarwal A. Modified Eshelby tensor modeling for elastic property prediction of carbon nanotube reinforced ceramic nanocomposites. Appl Phys Lett 2007;91(3):031903–031903-3.
[4] Hershey AV. The elasticity of anisotropic aggregate of an isotropic cubic crystals. J Appl Mech 1954;21:236–40.
[5] Christensen RM, Lo KH. Solutions for effective and shear properties in three phase and cylinder models. J Mech Phys Solids 1979;27:315–30.
[6] Hill RJ. A self-consistent mechanics of composite materials. J Mech Phys Solids 1965;13:213–22.
[7] Budiansky BJ. On the elastic moduli of some heterogeneous materials. J Mech Phys Solids 1965;13:223–7.
[8] Aboudi J, Arnold SM, Bednarcyk BA. Micromechanics of composite materials–a generalized multiscale analysis approach. Amsterdam: Elsevier; 2013.
[9] Lefik M, Boso DP, Schrefler BA. Generalized self-consistent homogenization using the finite element method. Z Angew Math Mech 2009;89:306–19.
[10] Boso DP, Lefik M, Schrefler BA. Generalized self-consistent like method for mechanical degradation of fibrous composites. Z Angew Math Mech 2011;91:967–78.
[11] Boso DP, Lefik M, Schrefler BA. Generalized self-consistent homogenization as an inverse problem. Z Angew Math Mech 2010;90:847–60.
[12] Atalay MA, Aydin ED, Aydin M. Multi-region heat conduction problems by boundary element method. Int J Heat Mass Transf 2004;47:1549–53.
[13] Dong CY. Boundary integral equation formulations for steady state thermal conduction and their applications in heterogeneities. Eng Anal Bound Elem 2015;54:60–7.
[14] Qin X, Zhang JM, Liu L, Li G. Steady-state heat conduction analysis of solids with small open-ended tubular holes by BEM. Int J Heat Mass Transf 2012;55:6846–53.
[15] Hughes TJ, Cottrell JA, Bazilevs Y. Isogeometric analysis: CAD, finite elements, NURBS, exact geometry and mesh refinement. Comput Methods Appl Mech Eng 2005;194:4135–95.
[16] Grebennikov AI. Isogeometric approximation of functions of one variable. USSR Comput Math Math Phys 1982;22(6):1323–30.
[17] Nguyen T, Jüttler B. Parameterization of contractible domains using sequences of harmonic maps. Curves Surfaces Int Conf 2010;6920:501–14.
[18] Xu G, Mourrain B, Duvigneau R, Galligo A. Constructing analysis-suitable parameterization of computational domain from CAD boundary by variational harmonic method. J Comput Phys 2013;252:275–89.
[19] Xu G, Mourrain B, Duvigneau R, Galligo A. Optimal analysis-aware parameterization of computational domain in 3D isogeometric analysis. Comput Aided Des 2013;45(4):812–21.
[20] Xu G, Mourrain B, Duvigneau R, Galligo A. Analysis-suitable volume parameterization of multi-block computational domain in isogeometric applications. Comput Aided Des 2013;45(2):395–404.
[21] Elisabeth P, Jüttler B. Bounding the influence of domain parameterization and knot spacing on numerical stability in isogeometric analysis. Comput Methods Appl Mech Eng 2014;268(1):589–613.
[22] Xu G, Atroshchenko E, Ma W, Bordas SPA. Geometry - independent field approximation for adaptive spline-based finite element methods. Proceedings of the 11th World Congress in Computational Mechanics. July 2014.
[23] Simpson RN, Bordas SPA, Trevelyan J, Rabczuk T. A two-dimensional isogeometric boundary element method for elastostatic analysis. Comput Methods Appl Mech Eng 2012;209:87–100.
[24] Simpson RN, Bordas SPA, Lian H, Trevelyan J. An isogeometric boundary element method for elastostatic analysis: 2D implementation aspects. Comput Struct 2013;118(6):2–12.
[25] Scott MA, Simpson RN, Evans JA, Lipton S, Bordas SPA, Hughes TJR, Sederberg TW. Isogeometric boundary element analysis using unstructured T-splines. Comput Methods Appl Mech Eng 2013;254:197–221.
[26] Lian H, Simpson RN, Bordas S. Stress analysis without meshing: isogeometric boundary-element method. Eng Comput Mech 2013;166(2):88–99.
[27] Xuan P, Atroshchenko E, Bordas S. Damage tolerance assessment directly from CAD: (extended) isogeometric boundary element methods (XIGABEM). https://orbilu.uni.lu/bitstream/10993/15768/1/acomen_template.pdf; 2014.
[28] Xuan P, Atroshchenko E, Simpson R, Kulasegaram S, Bordas S. Crack growth analysis by a NURBS-based isogeometric boundary element method. http://publications.uni.lu/bitstream/10993/14135/1/abstractWCCM.pdf; 2014.
[29] Lian H, Kerfriden P, Bordas SPA. Implementation of regularized isogeometric boundary element methods for gradient-based shape optimization in two-dimensional linear elasticity. Int J Numer Methods Eng 2016;106(12):972–1017.
[30] Lian H, Kerfriden P, Bordas SPA. Shape optimization directly from CAD: an isogeometric boundary element approach using T-splines. Comput Methods Appl Mech Eng 2017;317:1–41.
[31] Nguyen VP, Anitescu C, Bordas SPA, Rabczuk T. Isogeometric analysis: an overview and computer implementation aspects. Math Comput Simul 2015;117:89–116.
[32] Lian H, Bordas SPA, Sevilla R, Simpson RN. Recent developments in CAD/analysis integration. Mathematics 2012;6.
[33] Bordas SPA, Rabczuk T, Rodenas JJ, Kerfriden P, Moumnassi M, Belouettar S. Recent advances towards reducing the meshing and re-meshing burden in computational sciences. Comput Technol Rev 2010;2:51–82.
[34] Sevilla R, Fernández-Méndez S, Huerta A. NURBS-enhanced finite element method (NEFEM). Int J Numer Methods Eng 2008;76(1):56–83.
[35] Moumnassi M, Belouettar S, Béchet É, Bordas SPA, Quoirin D, Potier-Ferry M. Finite element analysis on implicitly defined domains: an accurate representation based on arbitrary parametric surfaces. Comput Methods Appl Mech Eng 2011;200(5):774–96.
[36] Legrain G, Geuzaine C, Remacle JF, Moës N, Cresta P, Gaudin J. Numerical simulation of CAD thin structures using the extended finite element method and level sets. Finite Elem Anal Des 2013;77:40–58.
[37] Legrain G, Chevaugeon N, Dréau K. High order X-FEM and level sets for complex microstructures: uncoupling geometry and approximation. Comput Methods Appl Mech Eng 2012;241:172–89.
[38] Legrain G. A NURBS enhanced extended finite element approach for unfitted CAD analysis. Comput Mech 2013;52(4):913–29.
[39] Nguyen-Thanh N, Nguyen-Xuan H, Bordas SPA, Rabczuk T. Isogeometric analysis using polynomial splines over hierarchical T-meshes for two-dimensional elastic solids. Comput Methods Appl Mech Eng 2011;200(21):1892–908.
[40] Schillinger D, Evans JA, Reali A, Scott MA, Hughes TJR. Isogeometric collocation: cost comparison with Galerkin methods and extension to adaptive hierarchical NURBS discretizations. Comput Methods Appl Mech Eng 2013;267:170–232.
[41] Simpson RN, Scott MA, Taus M, Thomas DC, Lian H. Acoustic isogeometric boundary element analysis. Comput Methods Appl Mech Eng 2014;269:265–90.
[42] Gong YP, Dong CY, Qin XC. An isogeometric boundary element method for three dimensional potential problems. J Comput Appl Math 2017;313:454–68.
[43] Gong YP, Dong CY. An isogeometric boundary element method using adaptive integral method for 3D potential problems. J Comput Appl Math 2017;319:141–58.
[44] Gao XW, Davies TG. Adaptive integration in elasto-plastic boundary element analysis. J Chin Inst Eng 2000;23(3):349–56.
[45] Peng X, Atroshchenko E, Kerfriden P, Bordas SPA. Isogeometric boundary element methods for three dimensional static fracture and fatigue crack growth. Comput Methods Appl Mech Eng 2017;316:151–85.
[46] Peng X, Atroshchenko E, Kerfriden P, Bordas SPA. Linear elastic fracture simulation directly from CAD: 2D NURBS-based implementation and role of tip enrichment. Int J Fracture 2017;204(1):55–78.
[47] Cirak F, Ortiz M, Schroder P. Subdivision surfaces: a new paradigm for thin-shell finite-element analysis. Int J Numer Methods Eng 2015;47(12):2039–72.
[48] Cirak F, Scott MJ, Antonsson EK, Ortiz M, Schröder P. Integrated modeling, finite-element analysis, and engineering design for thin-shell structures using subdivision. Comput Aided Des 2002;34(2):137–48.
[49] Hatta H, Taya M. Effective thermal conductivity of a misoriented short fiber composite. J Appl Phys 1985;58(7):2478–86.
[50] Dunn ML, Taya M, Hatta H, Takei T, Nakajima Y. Thermal conductivity of hybrid short fiber composites. J Compos Mater 1993;27(15):1493–519.
[51] Ali A, Rajakumar C. The boundary element method. Applications in sound and vibration. Crc Press; 2004.
[52] Dong CY, Lo SH, Cheung YK. Application of the boundary-domain integral equation in elastic inclusion problems. Eng Anal Bound Elem 2002;26:471–7.
[53] Beer G, Smith I, Duenser C. The boundary element method with programming for engineers and scientists. Wien, NewYork: Springer; 2008.
[54] Mustoe GGW. Advanced integration schemes over boundary elements and volume cells for two- and three-dimensional non-linear analysis. In: Banerjee PK, Mukherjee S, editors. Developments in boundary element methods - 3. London: Elsevier; 1984. p. 213–70.
[55] Davies TG, Bu S. Effective evaluation of non-singular integrals in 3D BEM. Adv Eng Software 1995;23:121–8.
[56] Gao XW, Davies TG. Boundary element programming in mechanics. Cambridge University Press; 2002.
[57] Dong CY. An interface integral formulation of heat energy calculation of steady state heat conduction in heterogeneous media. Int J Heat Mass Transf 2015;90:314–22.
[58] Christensen RM. Mechanics of composite materials. NewYork: Wiley; 1979.
[59] Gao XW. An effective method for numerical evaluation of general 2D and 3D high order singular boundary integrals. Comput Methods Appl Mech Eng 2010;199:2856–64.
[60] Lee YM, Yang RB, Gau SS. A generalized self-consistent method for calculation of effective thermal conductivity of composites with interfacial contact conductance. Int Commun Heat Mass Transf 2006;33:142–50.
[61] Hashin Z. The elastic moduli of heterogeneous materials. J Appl Mech 1962;29:143–50.
[62] Hashin Z. Analysis of composite materials-a survey. J Appl Mech 1983;50:481–505.